# Experimental Demonstration of Ordered and Disordered Multiresonant Metamaterials for Lamb Waves

Matthieu Rupin,[1] Fabrice Lemoult,[2] Geoffroy Lerosey,[2] and Philippe Roux[1,*]
[1]Institut des Sciences de la Terre, UMR 5275, Université Joseph Fourier, 38000 Grenoble, France
[2]Institut Langevin, ESPCI ParisTech and CNRS UMR 7587, PSL Research University, 1 rue Jussieu, 75005, Paris, France
(Received 11 February 2014; published 10 June 2014)

We demonstrate the experimental realization of a multiresonant metamaterial for Lamb waves, i.e., elastic waves propagating in plates. The metamaterial effect comes from the resonances of long aluminum rods that are attached to an aluminum plate. Using time-dependent measurements, we experimentally prove that this metamaterial exhibits wide band gaps as well as sub- and suprawavelength modes for both a periodic and a random arrangement of the resonators. The dispersion curve inside the metamaterial is predicted through hybridizations between flexural and compressional resonances in the rods and slow and fast Lamb modes in the plate. We finally underline how the various degrees of freedom of such system paves the way to the design of metamaterials for the control of Lamb waves in unprecedented ways.

DOI: 10.1103/PhysRevLett.112.234301 PACS numbers: 43.20.+g, 46.40.Cd, 46.40.Ff, 63.20.D-

Man-made composite materials have generated a wealth of studies in the community of wave physics over the past 20 years, as they can have properties that cannot be found in natural materials. It is now well accepted that the properties of these propagation media stem from two distinct origins: the ordered or disordered spatial distributions of their constituents, and the resonant or nonresonant nature of their unit cell [1,2]. When waves propagate in composite media with a structural order, they can undergo multiple scattering, which leads to frequency bands of permitted and prohibited propagation. These prohibited propagation bands (defined as band gaps) are analogous to electronic band gaps in natural crystals [3]. These materials have a typical spatial scale comparable to the wavelength at the frequencies of interest. They are termed photonic crystals in electromagnetics [4–6] and phononic crystals in acoustics [7–17] and constitute powerful tools to shape the flow of waves in various ways [6].

On the other hand, composite materials made out of resonant elements, also called locally resonant media, owe their macroscopic properties to the dispersive nature of their unit cell [1,18–25]. They can be organized at a smaller scale than the wavelength, in which case they belong to the family of metamaterials [26,27]. Metamaterials can have bands with high momentum modes that are equivalent to high effective parameters [20,28–30] or frequency bands with negative effective properties that manifest as band gaps [18,19,23,24,31–33]. In the absence of near-field coupling, the metamaterial properties can be interpreted from Fano interferences between the propagating and scattered waves; this leads to hybridization between local resonances and the incident waves that propagate in the host medium [24,34]. The spatial organization of the material is no longer relevant, and band gaps may be observed whether it is ordered or disordered [23,35].

The width and efficiency of band gaps in locally resonant metamaterials depend upon both the spatial density of the resonators and the quality factor of the resonance. Indeed, in the limit of small resonators compared to the wavelength, the smaller the resonator, the higher its quality factor. This justifies why locally resonant metamaterials classically support subwavelength modes and band gaps limited to narrow bandwidths. To overcome this fundamental limitation, a dimension of the physical space can be sacrificed by creating a uniaxial metamaterial [30,36,37], which consists of resonators that are small compared to the wavelength in 2D, while this restriction is relaxed in the third dimension [24]. One example is the so-called wire medium in electromagnetism, which has been used to control and/or focus waves below the diffraction limit [24,30,37]. In acoustics, a collection of narrow but long pipes was recently used to realize a super lens [38]. Although limited so far to 3D metamaterials, this approach is perfectly suited to 2D surface waves in acoustics and electromagnetism.

In this Letter, we demonstrate experimentally how uniaxial metamaterials present richer characteristics than any other metamaterials for Lamb waves [39–45]. To do so, we study a stadium-shaped metallic plate that behaves as an ergodic cavity for surface waves. A collection of long thin metallic rods is attached on a square portion of the plate. These rods are organized in a periodic or a random pattern, hence, providing an ordered or disordered Lamb wave metamaterial. The propagation of Lamb waves [46,47] inside and outside these metamaterials is then mapped across a large frequency spectrum. Interestingly enough, both the periodic and the random samples show identical wide band gaps for all of the angles of incidence. The ordered and disordered metamaterials also support sub- and suprawavelength modes for frequency bands on the edge of the band gaps. Finally, the dispersion relations of the metamaterials are

 

compared to numerical simulations. While the metamaterial effect usually comes from the hybridization of a single propagating mode with a single local resonance, we identify here the hybridizations of the slow ($A_0$) and fast ($S_0$) Lamb waves with the compressional and flexural resonances of the metallic rods.

The investigation of the uniaxial metamaterial for Lamb waves was made through experiments at a larger mesoscopic scale (and, hence, at a lower frequency) than usually reported in the literature. A 6-mm-thick and 1.5-m by 2-m-long aluminum plate was locally excited by a dynamic shaker with a 1.8-s-long broadband chirp that ranged from 500 Hz to 11 kHz [Fig. 1(a)]. At low frequency, two Lamb modes propagate in the plate, which are defined as the antisymmetric $A_0$ and the symmetric $S_0$ modes. The $A_0$ mode mostly corresponds to a vertical displacement of the plate, while the $S_0$ mode corresponds to a horizontal displacement. For symmetry reasons, the shaker only excites the $A_0$ mode [48], and only the vertical displacement of the plate is locally probed with the laser interferometer. The chaotic shape of the plate (Bunimovich stadium) ensures that, whatever the source position, the waves propagate at long time in all directions with equal probabilities [48–50]. Note that the $A_0$ Lamb waves have a quadratic dispersion relation [46–48] with typical wave speed of 340 m/s at 2 kHz (wavelength $\lambda = 17.5$ cm). The multiply reverberated waves are measured on the upper side of the plate, and after cross correlation with the emitted chirp, the plate response is spread over more than 200 ms [Fig. 1(b)], to be compared to the 1-ms-long autocorrelation signal. This corresponds to more than 20 round trips of the propagating waves across the plate. Using PC-controlled motorized mirrors, the vertical displacement of the plate surface can be scanned on a 0.20 m by 1.15 m surface $S$ [Fig. 1(a), rectangle numbered 5] with a resolution of 3 mm. This accurate estimation of the waves interference pattern created by the shaker in the plate is referred to in the following as the spatiotemporal wave field.

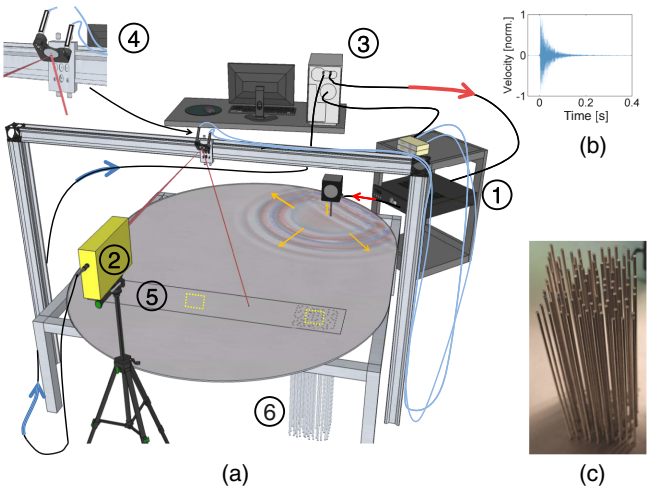


FIG. 1 (color online). (a) Experimental setup. A shaker (1) generates $A_0$ Lamb waves in the aluminum plate. The wave field is measured with a Doppler velocimeter (2) and a PC-controlled (3) motorized mirror(4) on the rectangular area (5) on the upper side of the plate. The metamaterial (6) is attached below the plate on one side of the recording map. (b) The typical temporal dispersion exceeds 0.2 s, which corresponds to more than 20 round-trips inside the plate. (c) The metamaterial is made of 100 vertical aluminium rods that can be arranged on a periodic or random pattern, with an average inter-rod distance of the order of 2 cm.

Within this scanned area, a metamaterial is built with a set of 100 cylindrical 61-cm-long, 6.35-mm-diameter aluminum rods glued on a 400 cm$^2$ area on the lower side of the plate [Fig. 1(c)]. Two different configurations were studied depending upon the random or periodic arrangement of the rods. The average distance between resonators is of the order of 2 cm (i.e., $\lambda/9$ and $\lambda/4$ for the $A_0$ mode at 2 and 10 kHz), which corresponds to a 2-cm-wide square lattice for the periodic sample. A 5-mm minimum inter-rod distance was used for the random arrangement. For Lamb waves, this collection of rods is equivalent to a set of subwavelength resonant scatterers exhibiting several resonances of different nature (longitudinal and flexural resonances of rods) in the frequency range under study.

When the plate vertical displacement is probed outside the metamaterial, the spatially averaged Fourier transform shows a maximum energy density below 2 kHz, followed by a plateau up to 11 kHz [Fig. 2(a), dashed gray curve]. The sudden 10-dB drop at 2 kHz is due to the radiation leakage of the $A_0$ Lamb mode in air [48]. At 2 kHz, the wave speed of the $A_0$ Lamb waves matches the sound velocity (≈340 m/s), and the plate radiates sound in air. This phenomenon necessitates an explanation but has no influence on the physics of the metamaterial. The Fourier spectrum measured above the multiresonator ordered and disordered metamaterials reveals three wide band gaps starting at 2, 6, and 10 kHz. The band gaps are similar in shape and intensity

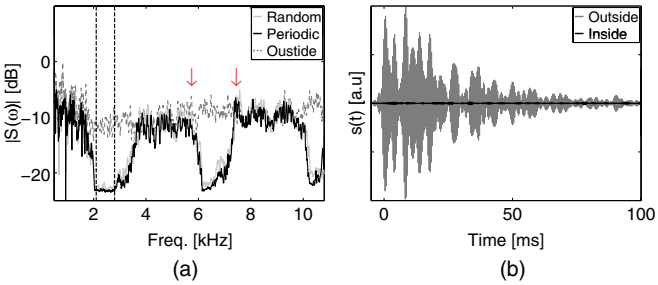


FIG. 2 (color online). (a) Average Fourier spectra for the signals measured inside (black line for the periodic sample, gray line for the random sample) and outside (dashed gray) the metamaterial. The averaging is performed over two surfaces marked as dotted squares within the rectangle measurement area (number 5) in Fig. 1. (b) Strongly reverberated signals are obtained outside the metamaterial after filtering in the first band gap [dashed vertical lines in (a)]. Both signals are measured at the center of the averaging areas described in (a).

independently of the periodic or random organization of the rods. This demonstrates that spatial disorder does not affect the properties of the metamaterial whose behavior cannot be explained with constructive or destructive interferences associated with Bragg scattering. Moreover, even at long reverberation times, the temporal response filtered within the first band gap [vertical dashed line in Fig. 2(a)] remains almost null in the metamaterial [Fig. 2(b)]. Since the plate shape is chaotic and, hence, ergodic, this means that the band gaps are conserved for all angles of incidence [48].

For the sake of novelty, we present in the following, the spatiotemporal wave field measured on the surface $S$ with the random metamaterial only. In Figs. 3(a) and 3(b), the wave field was filtered in the first band gap [dashed vertical lines in Fig. 2(a)] and then mapped after a propagation time of 3 ms (corresponding to the ballistic field) and 41 ms (for multireverberated Lamb waves). These "snapshots" reveal the following information. First, the band gap is efficient, as waves have been clearly attenuated within a small fraction of the $A_0$ mode wavelength. Second, the band gap is valid for all incident angles, as can be seen from the second snapshot with a superposition of incident plane waves in all directions.

The wave field is also mapped in Figs. 3(c) and 3(d) for two distinct frequencies that are chosen outside of the band gaps, respectively, before and after the second one [red arrows in Fig. 2(a)]. At 5805 Hz, the mode inside the metamaterial has a much smaller spatial scale compared to the $A_0$ mode in the homogeneous plate. On the contrary, a larger effective wavelength is observed at 7512 Hz. These maps show that, depending on the frequency, the designed metamaterial presents a lower or higher effective phase velocity than that of the homogeneous plate.

To quantify this effect, dispersion curves were computed from the spatiotemporal wave field measured in the metamaterial. For each measured point, the temporal signal is Fourier transformed and a 2D spatial Fourier transform of the wave field is then calculated. At each frequency, this 2D Fourier spectrum is transformed into a frequency–wave-number dispersion curve using a radial averaging process. The wave physics of the metamaterial is then summarized in a single dispersion relation that shows the real part of the wave vector and the corresponding attenuation length within the band gaps [Figs. 4(a) and 4(b)]. The dispersion relations of the $S_0$ (black) and $A_0$ (gray) Lamb modes in the homogeneous plate are superimposed.

Since both ordered and disordered metamaterials give similar results, their properties arise from the resonant nature of the rods. To prove this point, the horizontal and vertical displacements of the rod's free end were measured on one single isolated rod. Different resonant peaks are observed [Fig. 4(c)] corresponding to different types of resonance. The horizontal displacement of the rod (gray) shows flexural resonances of the rod, while the vertical displacement (black) reveals compressional (or elongation) resonances. As expected, the compressional resonances are

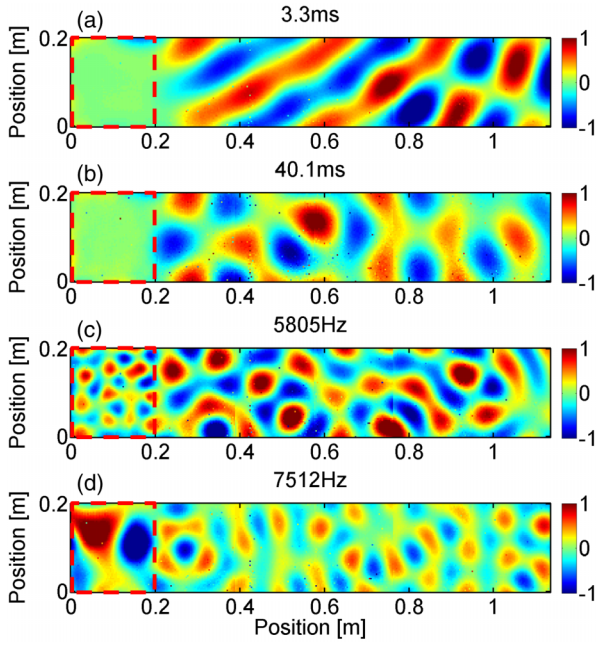


FIG. 3 (color online). Field maps on the rectangular area [see Fig. 1(a)] for the random metamaterial. (a),(b) Snapshots of the temporal field at 3 ms (a) and 41 ms (b) for signals filtered as in Fig. 2(b). (c),(d) Frequency-domain field maps at two frequencies before and after the second band gap, as indicated by the two red arrows in Fig. 2(a).

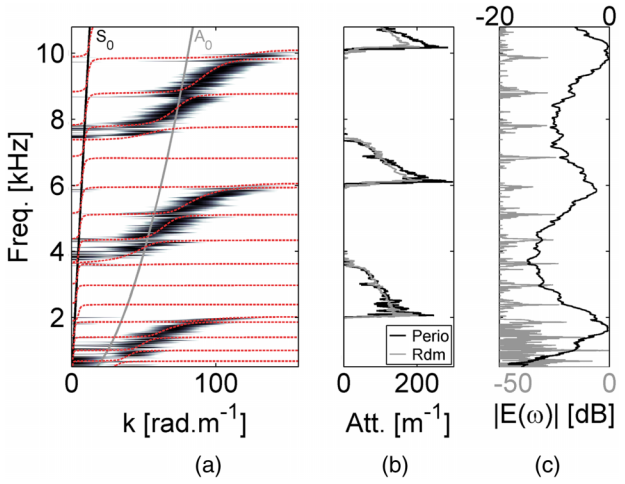


FIG. 4 (color online). (a) Frequency–wave-number representation of the wave field measured inside the random metamaterial. Theoretical dispersion curves for the homogeneous plate are superimposed: in black, the $S_0$ mode, and in gray, the $A_0$ one. The dashed curves correspond to the numerical dispersion curve for a periodic metamaterial using Bloch theorem. (b) Imaginary part of the $k$ vector measured inside the metamaterials for both the random (gray) and periodic (black) samples. (c) Frequency spectrum of the horizontal (gray) and vertical (black) displacements measured at the free end of one single isolated rod glued on the upper side of the plate.

linearly distributed over frequency while the flexural ones are quadratically distributed [47]. The individual response of one rod permits us to understand the dispersion relation of the metamaterial since each resonant peak corresponds to a specific behavior. At first, the $A_0$ mode of the plate strongly hybridizes with the compressional resonances, which gives rise to a polaritonic behavior at each crossing of the $A_0$ dispersion curve with these low-quality-factor resonances. Indeed, the vertical displacement of the $A_0$ mode efficiently couples with the compressional resonances resulting in the low $Q$ factor due to radiation leakage. As the metamaterial behavior results from Fano interference between the incoming waves and the scattered waves [24], the wide compressional resonances of the rods and their dense organization result in wide band gaps that start at the resonance and end at the antiresonance of one single rod. These band gaps show strong attenuations [Fig. 4(b)] that are insensitive to ordered or disordered configurations. Scaled at higher frequencies, these could be used to mold the flow of Lamb waves with applications to surface wave devices.

Outside the band gaps, the hybridizations between the $A_0$ mode and the rod compressional resonances give rise to two branches, namely, the antibinding branches and the binding ones. At frequencies above the band gaps, suprawavelength modes are observed [Fig. 3(d)]. On the contrary, the binding branches at frequencies below the band gaps are composed of subwavelength modes with spatial scales comparable to the average distance between rods [see Fig. 3(c)]. Thus, the designed metamaterials can be used for many different purposes. Indeed, as both suprawavelength and subwavelength modes can be efficiently excited on large frequency bandwidths within the metamaterials, it might be possible to tune the wave velocities, e.g., by shaping the length of the rods, so as to realize Lamb wave cloaks [51] or graded-index lenses [52,53]. Similarly, the subwavelength modes can be used alongside techniques such as time reversal in order to focus elastic waves onto very small spatial scales or to realize deep subwavelength sensors or actuators [20]. Note that these modes and the associated band gaps could be analyzed in the light of homogenization with effective parameters for Lamb waves, independent of their ordered or disordered arrangements.

More-subtle information can also be gained from the dispersion relation plotted in Fig. 4(a). Indeed, weaker hybridizations can be distinguished, the most visible around 4.3 or 8.7 kHz. These are related to flexural resonances of the rods, as indicated in Fig. 4(c). Flexural resonances are a consequence of the transverse displacement of the rods, and they can hybridize both with the $A_0$ and the $S_0$ modes. Stated differently, the plate modes created by the hybridization of the $A_0$ modes with the compressional resonances of the rods can hybridize again with the flexural resonances, hence, leading to an unusually rich behavior. This effect spans a narrow frequency range compared to the measured band gaps in agreement with the fact that flexural resonances have higher $Q$ factors. With both flexural and compressional resonances hybridizing with $A_0$ and $S_0$ Lamb modes in the plate, metamaterials made of uniaxial subwavelength resonators fastened to a 2D elastic plate reveal much richer physics than their acoustic or electromagnetic counterparts.

Finally, finite-element simulations were performed for an infinite equivalent (ordered) metamaterial using Bloch periodic boundary conditions applied to a unit cell made of one rod attached at the center of a 2 cm by 2 cm elastic plate. The numerical dispersion relation is superimposed onto the experimental one in Fig. 4(a) (red dashed lines). The good match confirms that the experimental random metamaterial behaves like the infinite and periodic simulated one. Moreover, the simulation gives information that was missing in the experiment. The $A_0$ mode, indeed, hybridizes with both the compressional and flexural resonances of the rods, giving rise to complex branches with two inflexions, while the $S_0$ mode only hybridizes with the flexural ones, as a signature of its symmetry. This shows that many degrees of freedom can be used to design Lamb wave metamaterials. Indeed, the rod length can first be modified to adjust the compressional resonance frequencies and, hence, modify the frequency range of the band gaps. Furthermore, the symmetry of the resonators can be changed using identical rods on each side of the plate, for instance, to forbid the conversion between the $A_0$ and $S_0$ modes. Finally, we noticed that using a thinner (and, thus, more flexible) plate leads to a more efficient excitation of both the compressional and flexural resonances of the rods. These practical aspects will be the scope of future works.

To conclude, we have experimentally studied ordered and disordered Lamb wave metamaterials built from long metallic rods perpendicularly attached to a thin metallic plate. Spatiotemporal maps of the wave field inside and outside the metamaterials were measured on a frequency spectrum that spanned about a decade. Through this experiment and the equivalent numerical simulations, these composite media were shown to support sub- and suprawavelength modes, as well as wide band gaps. The wave field properties do not depend on the spatial arrangement of the resonators inside the metamaterial. The metamaterial physics is explained through hybridizations between the $A_0$ and $S_0$ plate modes with the flexural and compressional resonances of the rods. This work paves the way to the design of metamaterials allowing an unprecedented control of Lamb wave propagation.

G. L. acknowledges funding from the French ANR under reference PLATON; G. L. and F. L. were partially supported by LABEX WIFI (Laboratory of Excellence ANR-10-LABX-24) within the French Program "Investments for the Future" under reference ANR-10-IDEX-0001-02 PSL*.

*Corresponding author.
Philippe.roux@ujf-grenoble.fr

[1] P. Deymier, *Acoustic Metamaterials and Phononic Crystals* (Springer, Berlin, 2013).
[2] M. Sigalas, M. S. Kushwaha, E. N. Economou, M. Kafesaki, I. E. Psarobas, and W. Steurer, Z. Kristallogr. **220**, 757764 (2009).
[3] C. Kittel, *Introduction to Solid State Physics* (Wiley, New York, 1996).
[4] E. Yablonovitch, Phys. Rev. Lett. **58**, 2059 (1987).
[5] S. John, Phys. Rev. Lett. **58**, 2486 (1987).
[6] J. D. Joannopoulos, S. G. Johnson, J. N. Winn, and R. D. Meade, *Photonic Crystals: Molding the Flow of Light* (Princeton University Press, Princeton, NJ, 2008).
[7] R. Martinez-Sala, J. Sancho, J. V. Sanchez, J. Linres, and F. Mesegure, Nature (London) **378**, 241 (1995).
[8] J. O. Vasseur, P. A. Deymier, B. Djafari-Rouhani, Y. Pennec, and A. C. Hladky-Hennion, Phys. Rev. B **77**, 085415 (2008).
[9] M. M. Sigalas and E. N. Economou, Solid State Commun. **86**, 141 (1993).
[10] S. Benchabane, A. Khelif, J.-Y. Rauch, L. Robert, and V. Laude, Phys. Rev. E **73**, 065601 (2006).
[11] J. H. Page, A. Sukhovich, S. Yang, M. Cowan, F. V. D. Biest, A. Tourin, M. Fink, Z. Liu, C. Chan, and P. Sheng, Phys. Status Solidi (b) **241**, 3454 (2004).
[12] A. Sukhovich, B. Merheb, K. Muralidharan, J. Vasseur, Y. Pennec, P. Deymier, and J. Page, Phys. Rev. Lett. **102**, 154301 (2009).
[13] M. Farhat, S. Guenneau, S. Enoch, A. B. Movchan, and G. G. Petursson, Appl. Phys. Lett. **96**, 081909 (2010).
[14] A. A. Maznev, O. B. Wright, and O. Matsuda, New J. Phys. **13**, 013037 (2011).
[15] A. Khelif, A. Choujaa, B. Djafari-Rouhani, M. Wilm, S. Ballandras, and V. Laude, Phys. Rev. B **68**, 214301 (2003).
[16] J. Pierre, O. Boyko, L. Belliard, J. O. Vasseur, and B. Bonello, Appl. Phys. Lett. **97**, 121919 (2010).
[17] M. Dubois, M. Farhat, E. Bossy, S. Enoch, S. Guenneau, and P. Sebbah, Appl. Phys. Lett. **103**, 071915 (2013).
[18] Z. Liu, X. Zhang, Y. Mao, Y. Y. Zhu, Z. Yang, C. T. Chan, and P. Sheng, Science **289**, 1734 (2000).
[19] N. Fang, D. Xi, J. Xu, M. Ambati, W. Srituravanich, C. Sun, and X. Zhang, Nat. Mater. **5**, 452 (2006).
[20] F. Lemoult, M. Fink, and G. Lerosey, Phys. Rev. Lett. **107**, 064301 (2011).
[21] V. Leroy, A. Strybulevych, M. Scanlon, and J. H. Page, Eur. Phys. J. E **29**, 123 (2009).
[22] I. E. Psarobas, A. Modinos, R. Sainidou, and N. Stefanou, Phys. Rev. B **65**, 064307 (2002).
[23] M. L. Cowan, J. H. Page, and P. Sheng, Phys. Rev. B **84**, 094305 (2011).
[24] F. Lemoult, N. Kaina, M. Fink, and G. Lerosey, Nat. Phys. **9**, 55 (2013).
[25] J. Christensen and F. J. G. de Abajo, Phys. Rev. Lett. **108**, 124301 (2012).
[26] J. B. Pendry, A. J. Holden, D. J. Robbins, and W. J. Stewart, IEEE Trans. Microwave Theory Tech. **47**, 2075 (1999).
[27] D. R. Smith, W. J. Padilla, D. C. Vier, S. C. Nemat-Nasser, and S. Schultz, Phys. Rev. Lett. **84**, 4184 (2000).
[28] J. T. Shen, P. B. Catrysse, and S. Fan, Phys. Rev. Lett. **94**, 197401 (2005).
[29] M. Choi, S. H. Lee, Y. Kim, S. B. Kang, J. Shin, M. H. Kwak, K. Y. Kang, Y. H. Lee, N. Park, and B. Min, Nature (London) **470**, 369 (2011).
[30] F. Lemoult, G. Lerosey, J. d. Rosny, and M. Fink, Phys. Rev. Lett. **104**, 203901 (2010).
[31] J. Li and C. T. Chan, Phys. Rev. E **70**, 055602 (2004).
[32] J. H. Page, E. J. S. Lee, and C. Croenne, J. Acoust. Soc. Am. **134**, 4026 (2013).
[33] C. Inserra, V. Tournat, and V. Gusev, Europhys. Lett. **78**, 44001 (2007).
[34] N. Kaina, M. Fink, and G. Lerosey, Sci. Rep. **3**, 3240 (2013).
[35] N. Kaina, F. Lemoult, M. Fink, and G. Lerosey, Appl. Phys. Lett. **102**, 144104 (2013).
[36] F. Lemoult, M. Fink, and G. Lerosey, Wave Random Complex **21**, 591 (2011).
[37] P. A. Belov, Y. Hao, and S. Sudhakaran, Phys. Rev. B **73**, 033108 (2006).
[38] J. Zhu, J. Christensen, J. Jung, L. Martin-Moreno, X. Yin, L. Fok, X. Zhang, and F. J. Garcia-Vidal, Nat. Phys. **7**, 52 (2010).
[39] Y. Pennec, B. Djafari Rouhani, H. Larabi, A. Akjouj, J. N. Gillet, J. O. Vasseur, and G. Thabet, Phys. Rev. B **80**, 144302 (2009).
[40] T.-C. Wu, T. -T. Wu, and J.-C. Hsu, Phys. Rev. B **79**, 104306 (2009).
[41] A. Khelif, Y. Achaoui, S. Benchabane, V. Laude, and B. Aoubiza, Phys. Rev. B **81**, 214303 (2010).
[42] M. Oudich, M. Senesi, M. Assouar, M. Ruzenne, J. Sun, B. Vincent, Z. Hou, and T.-T. Wu, Phys. Rev. B **84**, 165136 (2011).
[43] M. Assouar, M. Senesi, M. Oudich, M. Ruzzene, and Z. Hou, Appl. Phys. Lett. **101**, 173505 (2012).
[44] Y. Xiao, J. Wen, and X. Wen, J. Phys. D **45**, 195401 (2012).
[45] J. -C. Hsu, J. Phys. D **46**, 015301 (2013).
[46] H. Lamb, Proc. London Math. Soc. **s2-1**, 473 (1904).
[47] D. Royer and E. Dieulesaint, *Elastic Waves in Solids I: Free and Guided Propagation* (Springer, Berlin, 2000).
[48] See Supplemental Material at http://link.aps.org/supplemental/10.1103/PhysRevLett.112.234301 for (i) dispersion relation of Lamb waves; (ii) excitation with the shaker; (iii) definition of ergodicity; (iv) coupling between $A_0$ Lamb waves and airborne acoustic waves.
[49] M. C. Gutzwiller, *Chaos in Classical and Quantum Mechanics* (Springer–Verlag, New York, 1990).
[50] L. A. Bunimovich, Commun. Math. Phys. **65**, 295 (1979).
[51] M. Farhat, S. Guenneau, and S. Enoch, Phys. Rev. Lett. **103**, 024301 (2009).
[52] T. T. Wu, Y. T. Chen, J. H. Sun, S. C. S. Lin, and T. J. Huang, Appl. Phys. Lett. **98**, 171911 (2011).
[53] J. Zhao, R. Marchal, B. Bonello, and O. Boyko, Appl. Phys. Lett. **101**, 261905 (2012).